Check for updates

Dual impact of water on stability of metal–organic frameworks

Fatemeh Keshavarz [ID] *

The widespread application of metal–organic frameworks (MOFs) is hindered by their hydrolytic instability in aqueous and humid environments. To overcome this bottleneck, herein, we evaluate four representative MOFs−MOF-303 (highly stable), MIL-127(Fe) (stable), HKUST-1 (moderately unstable), and UMCM-1 (unstable) − using periodic and fragment-based density functional theory. By distinguishing the water adsorption, condensation, and hydrolysis pathways, we identify the structural and chemical factors that govern stability. Our results reveal the dual impact of water: it can destabilize frameworks by facilitating metal–ligand bond cleavage and improving ligand–ligand interactions of detached linkers, as in UMCM-1 and HKUST-1, but can also enhance stability by forming extended hydrogen-bond networks with polar ligands, as observed in MOF-303. This cooperative water–ligand interaction shields metal–oxygen bonds and prevents pore collapse, challenging the prevailing view that hydrophobicity is key to promoting stability. These insights clarify contradictory experimental reports and establish general design principles, highlighting that water is both a threat and a stabilizer depending on the framework's connectivity and ligand chemistry.

1. Introduction

Metal–organic frameworks (MOFs) are promising candidates for many diverse applications because their properties can be easily tailored by the right choice of metal nodes and organic linkers.[1,2] They can also be modified by adding metal clusters and organic compounds into their pores.[3] Also, many MOFs present highly crystalline and porous structures with high surface areas.[1–3] All these have resulted in the fast development of numerous MOFs for applications ranging from catalysis[4] to gas capture,[5] water treatment[6] and atmospheric water harvesting.[7] However, some shortcomings of MOFs have prevented their widespread industrial application and commercialization.

A major shortcoming is MOFs' instability under humid and aqueous conditions.[8] This is a major concern because the feeds of many industries contain moisture, and some MOF applications, such as water treatment and atmospheric water harvesting, involve aqueous or condensed water. Under such operational conditions, many MOFs undergo hydrolysis and degrade. To prevent hydrolysis and promote industrial adoption of MOFs, we need to understand and promote the water stability of MOFs. However, the hydrolysis process is poorly understood.

Department of Physics, School of Engineering Science, LUT University,
Yliopistonkatu 34, FI-53850, Lappeenranta, Finland.
E-mail: fatemeh.keshavarz@lut.fi

The process is generalized as an event that occurs at the bonds between the metal centers (M) and organic ligands (L) through reactions (R1) and (R2):[9]

$$L_xM^{n+}{-}^{-}(O_2C){-}R + H_2O \rightarrow L_xM^{n+}{-}^{-}(OH) + R{-}(CO_2H) \quad (R1)$$

$$L_xM^{n+}{-}^{-}(O_2C){-}R + H_2O \rightarrow [L_xM^{n+}{-}(OH_2)]^+ + R{-}(CO_2)^- \quad (R2)$$

In reaction (R1), the water molecule breaks, adds a hydroxyl group to the metal center and hydrogenates the organic linker. In reaction (R2), the water directly inserts into the metal-linker bond and the deprotonated organic ligand releases. Therefore, the strength of the M–L bond, steric hindrance and dense connectivity around the metal node and hydrophobicity are suggested to improve the water stability of MOFs.[9–11] These key properties have been exemplified by several experimental studies[12–15] and contradicted by some others.[16–21,22]

To provide a more robust guideline for finding water-stable MOFs, Batra *et al.*[23] and Terrones *et al.*[22] developed machine learning based models and identified some important features through importance analyses. The positively effective features recommended by Batra *et al.*[23] included the presence of metal ions with an atomic radius larger than 1.4 Å and an ionization potential lower than 7.5 eV and ligands featuring a high number of cyclic divalent nodes and fewer six-membered rings. The features distinguished by Terrones *et al.*[22] included the nuclear charge of the metals and the atoms involved in the three atoms bonded with each other and connected to the metals and high differences in the electronegativities of the metals and the two atoms next to the metals. Also, Yang and

This journal is © the Owner Societies 2026

Phys. Chem. Chem. Phys., 2026, **28**, 6089–6098 | **6089**

Gates correlated metal node coordination with water stability.[24] These features and correlations reflect on the outlined general guideline but give a more specific picture of the effective parameters in water hydrolysis.

Furthermore, some studies have conducted atomic simulations to understand the hydrolysis mechanisms of some MOFs under different conditions, for example, HKUST-1,[25,26] Ni-MOF-74,[27] MOF-5 (or Zn-IRMOF-1),[28–30] unsaturated $M_3(BTC)_2$,[31] NU-1000,[32] and DMOF-1.[33] These studies have provided valuable details on the reaction pathways. However, the fundamentals of MOF water stability remain poorly understood. To enhance our understanding of the impact of water on various MOFs, herein, we focus on four MOFs representing four categories of MOF water stability, *i.e.*, MOF-303 (high kinetic stability), MIL-127(Fe) (stable), HKUST-1 (low kinetic stability) and UMCM-1

(unstable). These MOFs are selected semi-randomly from the water stability data set reported by Burtch *et al.*[8] based on the availability of their crystal structure and the chemical diversity of their metal nodes. Among these MOFs, the hydrolysis process of HKUST-1 has been studied at the molecular level.[25,26] We use the corresponding molecular-level insight, try to reproduce and discuss their findings, and evaluate the hydrolysis of the MOFs. For thorough evaluations, we use periodic and model-based density functional theory calculations and a systematic configurational sampling approach[34,35] to study the adsorption of single water molecules, water condensation and the starting steps of water reaction with the MOFs. The MOF models are shown in Fig. 1, and the computational details are presented in Section S1 of the SI.
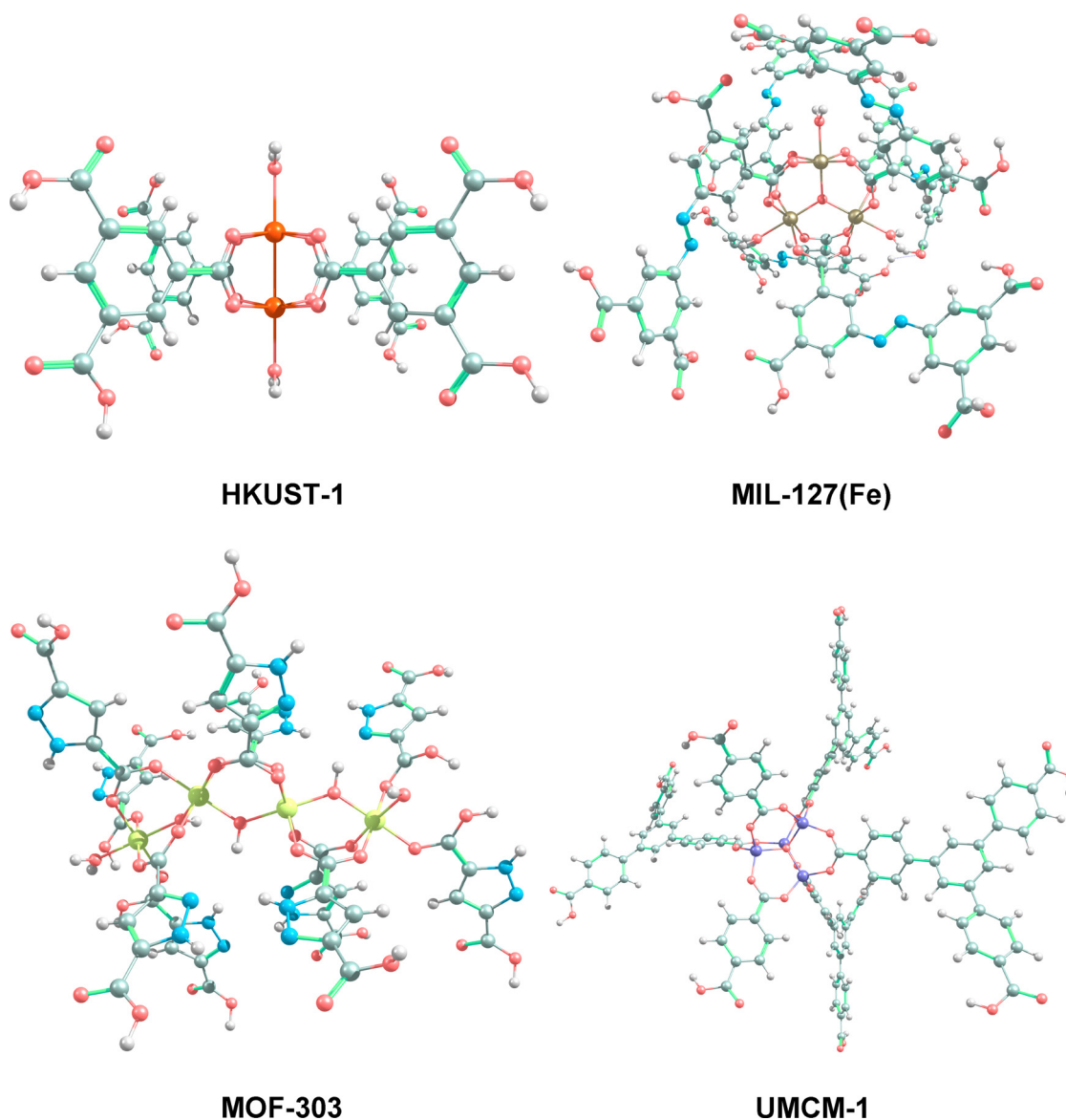

Fig. 1 The adopted MOF models for water adsorption and condensation studies. The orange, dark yellow, yellow, purple, red, blue, grey and white spheres represent the Cu, Fe, Al, Zn, O, N, C and H atoms, respectively.

6090 | *Phys. Chem. Chem. Phys.*, 2026, **28**, 6089–6098

This journal is © the Owner Societies 2026

2. Results and discussion

2.1 Water adsorption

As water uptake and hydrolysis processes start with the adsorption of a single water molecule into the MOF pores, we are concerned about the adsorption of first water molecules. Depending on the chemical nature of the ligands and the metal nodes, and also the availability of diffusion pathways/steric hindrance,[9,36] the first water molecules adsorb onto the site that offers the best adsorption efficiency. Particularly, a fully dehydrated/activated structure with open metal sites has vacant adsorption sites on their metal nodes to offer. For instance, HKUST-1 has two open Cu^{2+} sites. Each open Cu^{2+} site attracts one water molecule, binds to it axially, and creates a primary adsorption site for water (Fig. 1 and 2).[37–39] Such sites are so hydrophilic that HKUST-1 easily adsorbs water[37] and introduces structural water to its crystal.[40] The energy of adsorption (E_{ad}) (and Gibbs free energy of adsorption at 298.15 K and 1 atm; G_{ad}) per axial water molecule for the HKUST-1 model is −48.0 (−31.2) and −41.2 (−24.2) kJ mol^{-1} in the triplet and

singlet spin states, respectively. These E_{ad} values are consistent with the −45.6 kJ mol^{-1} value reported for the adsorption of a single axial water molecule by the HKUST-1 paddlewheel[41] and the results obtained from our periodic simulations (without zero-point energy correction), *i.e.* −54.6 kJ mol^{-1}. Also, the G_{ad} of the singlet state is slightly different from the −19.1 kJ mol^{-1} value reported at the B3LYP/def2SVP + SDD level of theory.[26] After full hydration of the metal nodes, the first guest water molecule interacts with carboxylate oxygen from the MOF linker and the hydrogen atom of an axial water molecule, as depicted in Fig. 2.

Like HKUST-1, MIL-127(Fe) presents three open Fe^{3+} sites, which adsorb three water molecules (Fig. 1 and 2). These sites are highly prone to water adsorption, with an average E_{ad} (G_{ad}) of −45.2 (−32.8) kJ mol^{-1} per axial water molecule for the fragment-based model. The removal of spin constraint and the application of periodic boundary conditions reduce the E_{ad} to −91.4 kJ mol^{-1} (excluding zero-point energy correction), which is significantly lower than that of HKUST-1 (−45.6 kJ mol^{-1}). The difference between the adsorption energies of the cluster
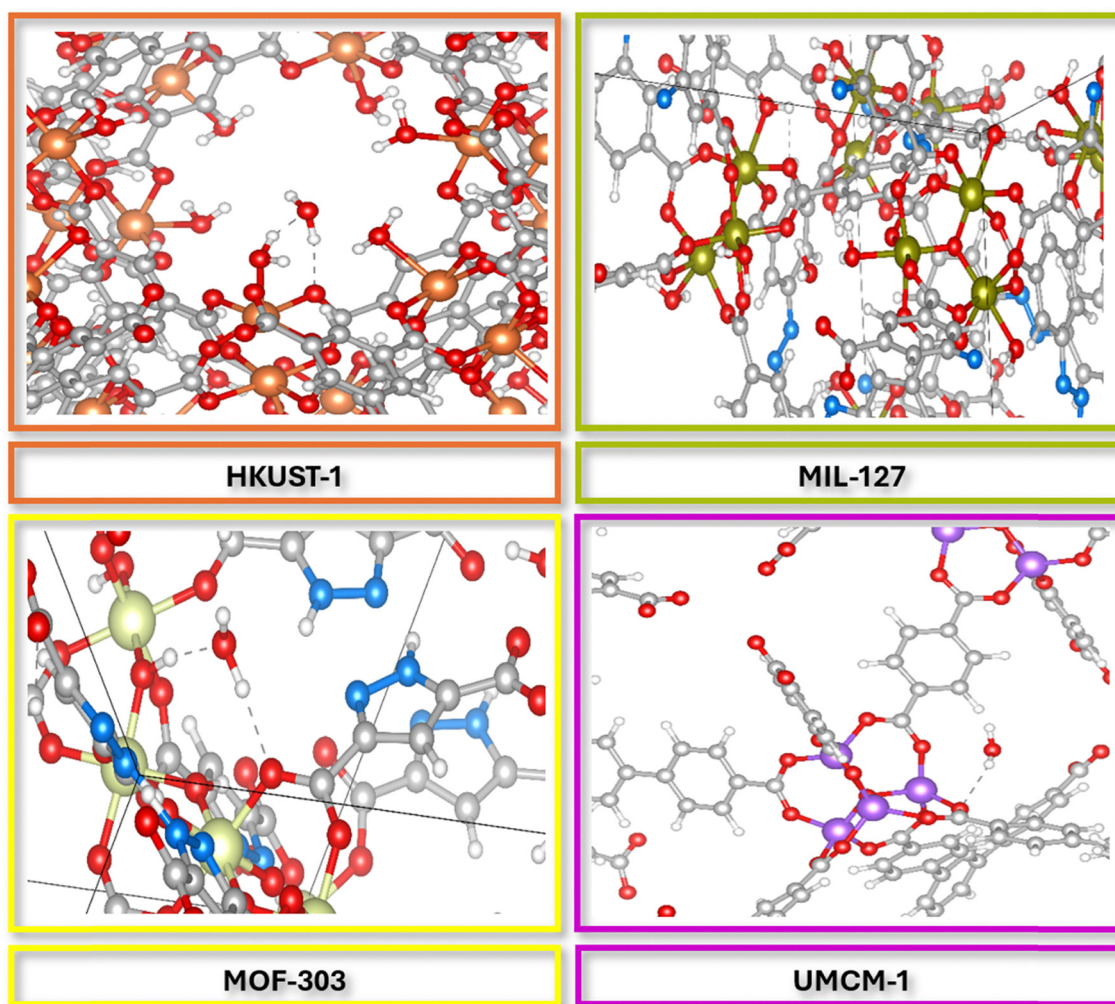

Fig. 2 Water adsorption onto the periodic MOF structures. The orange, dark yellow, light yellow, purple, red, blue, light grey and white spheres represent the Cu, Fe, Al, Zn, O, N, C and H atoms, respectively.

This journal is © the Owner Societies 2026

Phys. Chem. Chem. Phys., 2026, **28**, 6089–6098 | **6091**

and periodic models of MIL-127(Fe) arise from the entropy and structural variations induced by water. The periodic structure is more rigid, and its ligands cannot reorganize freely upon water adsorption. As a result, the adsorption process is mostly a local coordination process. In contrast, the unconstrained ligands of the truncated cluster model have additional degrees of freedom, which can rearrange and partially close the pore opening (Fig. 1) in the presence of axial water. The partial restructuring not only results in an enthalpic change of -46.2 kJ mol^{-1} but also leads to the significant entropy penalty (S_{ad}) of -44.9 J mol^{-1} K^{-1} (at temperature $T = 298.15$ K; $T.S_{ad} = -13.4$ kJ mol^{-1}). This flexibility and thermal/entropic contributions are the origins of the larger $|E_{ad}|$ values observed for the periodic model. After filling the unoccupied metal sites by axial water, the MOF adsorbs a guest water near their metal node through interaction with their linker's carboxylate oxygen. The interaction strengthens the interaction of the linker's second carboxylate oxygen with the neighboring axial water and tilts the axial water toward the ligand (Fig. 2).

An important fact is that the hydrophilicities of various open metal sites incorporated in different frameworks are not the same. Moreover, the structural and chemical properties of metal nodes impact their mode of water adsorption. For example, UMCM-1 has four Zn^{2+} sites to accommodate water. However, according to the configurational sampling results (Fig. S1) and the periodic simulations (Fig. 2), it does not adsorb water axially and it does not create octahedral metal coordination. Instead, the water molecule approaches the metal node by hydrogen bonding with a linker's carboxylate oxygen and interacting with a second ligand (Fig. 2). When the water molecule binds to the Zn^{2+} atom of the cluster model, it distorts the structure and converts the tetrahedral Zn center into a square pyramidal geometry, forcing the carboxylate oxygens into a spatial plane and hydrogen bonding with the carboxylate oxygen of a second Zn^{2+} center (Fig. S1). These changes, in addition to the tendency of the ligands toward π–π interactions, improve ligand–ligand interactions and facilitate their stacking on each other. When the ligands are fixed in the periodic MOF structure, the metal-bound ligands no longer move freely. This restriction prevents the π–π stacking and does not permit water to easily bind to the metal centers (Fig. 2). As a result, the periodic structure shows poor water adsorption, while the isolated cluster model adsorbs water more strongly ($E_{ad} = -177.5$ kJ mol^{-1} and $G_{ad} = -85.5$). The large difference between E_{ad} and G_{ad} does not arise from unusually strong binding, but from the increased conformational flexibility of the truncated ligands in the cluster model. When the extended lattice constraints are removed, the cluster undergoes substantial structural reorganization upon water adsorption, which results in both a larger enthalpic stabilization and a significant entropic penalty. Specifically, the adsorption enthalpy change is -186.3 kJ mol^{-1} and the entropy contribution is -338.2 J mol^{-1} K^{-1} (at 298.15 K; $T.S_{ad} = -100.8$ kJ mol^{-1}). Thus, the difference between E_{ad} and G_{ad} is almost entirely explained by the large entropy term, which is characteristic of flexible molecular clusters. In contrast, the periodic model

remains structurally rigid and therefore does not exhibit this entropy-driven energetic response.

In contrast to HKUST-1, MIL-126 and UMCM-1, MOF-303 does not offer any open metal sites. However, it presents multiple N, N–H, carboxylic oxygen, and bridging μ_2–OH sites to provide hydrogen bonding. Based on our configurational sampling results (Fig. S1), the first water molecule occupies the space between a μ_2–OH site (O$_{water}$–O$_\mu$ = 1.80 Å) and the nearest N–H and N (pyrazole) moieties (O$_{water}$–H(N) = 1.54 Å). The nearest free carboxylate group also contributes to the stabilization of the water molecule by rotating toward it. However, in the periodic structure (Fig. 2), the carboxylate groups are restrained, and the organic ligand cannot rotate without Al–O bond cleavage. Therefore, the water molecule stabilizes by establishing a hydrogen bond with an Al^{3+} bound carboxylate oxygen (H$_{water}$–O$_{ligand}$ = 1.82 Å) and a μ_2–OH site (O$_{water}$–O$_\mu$ = 2.74 Å). These adsorption modes share some features with the primary adsorption site reported by Chedda et al.,[42] who used Monte Carlo simulations and reported the formation of a hydrogen bond with the pyrazole NH and N functionalities and the bridging μ_2–OH, with O$_{water}$–O/N distances ranging from 2.7 to 3.0 Å. However, they have some differences. The observed differences are not essentially because of simulation errors or the use of a fragmented model. They mainly root in the high number of hydrophilic sites in MOF-303. All these sites are available for water adsorption and lead to impressive water uptake by MOF-303.[43] Based on the molecular dynamics simulations performed during our study, the water molecule moves dynamically between the Al–O and pyrazole sites. Therefore, we believe that there is no single "best" adsorption site for the water molecules and water moves freely between the available adsorption sites. However, it clearly prefers the O/H and N/H functionalities over direct binding to the Al^{3+} metals and the carbon moieties. The different adsorption modes and simulation methods result in the E_{ad} (G_{ad}) values of -177.2 (-104.5), -75.5, and -90 to -80[42] kJ mol^{-1} for the fragmented model, periodic DFT and Monte Carlo-based structures, respectively.

2.2 Water condensation

After the adsorption of the axial and the first non-axial water molecules, more water molecules can adsorb onto the MOFs. As water favors hydrogen bonding and the creation of a water network inside MOFs, the adsorption mode of the first molecule impacts the distribution of the others in the pores and the subsequent pore filling.[9] This is demonstrated by the configurational sampling results, in Fig. S1 and S2. For triplet HKUST-1 (Fig. S2), whose starting model contains axially coordinated water molecules, the axial water molecules and carboxylate oxygens play important roles in water condensation. The guest water molecule bridges between one axial water and a semi-detached carboxylate atom and the opposite end of the carboxylate ligand. This adsorption mode mimics the mode proposed by Xue et al.[26] and the mode observed in Fig. 2. The created water center seeds further water adsorption through hydrogen bonding and extends the network of water toward the space above the opposite ligands and then the space between

6092 | *Phys. Chem. Chem. Phys.*, 2026, **28**, 6089–6098

This journal is © the Owner Societies 2026

the ligands. This means that the water molecules avoid the hydrophobic space between the benzene rings of the carboxylate ligands unless there is another water molecule to help stabilize them through hydrogen bonding. The created water strings force the free ends of the ligands to move closer and create a tighter space between the ligands. Singlet HKUST-1 (Fig. S2) follows a rather similar trend of water condensation. However, it tends to delocalize the generated water cluster seeds to extend the water network from more directions.

MIL-126(Fe) has more axial water molecules and larger carboxylate ligands relative to HKUST-1, and its ligands can rotate and fold around their –N=N– moieties. These differences affect its water condensation mechanism, as depicted in Fig. S1. The first non-axial guest water molecule forms hydrogen bonds with two opposite carboxylate oxygen atoms, rather similar to the adsorption mode shown in Fig. 2. It also induces a conformational change in its surrounding free-ended ligands to effectively interact with their carboxylate ends. This results in a slight pore closure and collapsing of its ligands around the water molecule. The next water molecules adsorb onto the terminal carboxylate groups or enter the relatively enclosed pore and extend above the ligands similar to the case of HKUST-1. The preference of the MOF toward hydrogen bonding with more water molecules and the creation of a water wire overcomes the conformational freedom of the unrestrained ligands, resulting in pore opening in the presence of 8 guest water molecules. However, after that, the entrance of more water molecules re-induces pore closure.

The condensation of water onto the UCMC-1 model also causes some pore closure (see Fig. S1) because its extended carboxylate ligands with multiple benzene rings have a high potency for π–π stacking. The π–π interactions are observed as soon as the first water molecules adsorb onto the metal node by binding to the Zn atoms. The next water molecules bridge over the metal-bound water molecules and carboxylate atoms, all around the metal node and far from the hydrophobic ligand centers.

Though MOF-303 has many structural differences with the other MOFs, it exhibits some level of pore changes, as well. As aforementioned, this highly hydrophilic structure can adsorb water at different sites. As it interacts with the first water, a terminal ligand reorients toward the guest water molecules (Fig. S1). The forthcoming water molecules either form a hydrogen bond with the available water molecules or adsorb onto another free site. As water condensation continues, the different water clusters connect to each other and fill the pore. When the MOF space between two sets of ligands is unoccupied, π–π stacking occurs between the unrestrained imidazole rings. However, the filling of the MOF channels by water does not permit π–π stacking and helps the water molecules to enhance their interactions with the MOF's ligands.

All these results highlight the role of hydrogen bonding and hydrophilicity in shaping the behavior of water inside MOFs. They also clarify the general strengths and limitations of fragment-based cluster models. Because the truncated ligands

in these models are not fully constrained by the extended lattice, they retain a degree of conformational flexibility that is suppressed in intact periodic structures. In defect-free MOFs, coordination to the metal nodes restricts such motion. However, under conditions where defects or partial hydrolysis generates under-coordinated linkers, ligand mobility becomes relevant. In this sense, the cluster models capture the local chemistry around the metal nodes and also provide insight into how ligand flexibility may influence the early stages of structural destabilization under hydrolytic conditions. While the clusters are not intended to reproduce the full rigidity of the periodic frameworks, they are effective in identifying the qualitative trends and mechanistic pathways at the DFT level.

In addition to mechanistic insights, our results provide stepwise and total adsorption energies throughout the condensation process. The energy values (reported in Table S1) indicate that the adsorption of more water molecules is not necessarily a spontaneous process. For example, in the case of triplet HKUST-1, the adsorption of two additional water molecules onto the structure hosting 8 guests is not spontaneous. However, the continuation of the condensation, after that step, is spontaneous. Also, the results indicate that the process continues even though some of its steps are not thermodynamically as favorable as the others. There is no direct relationship with the number of water molecules and the average or stepwise adsorption energies.

2.3 Hydrolytic stability

When water is adsorbed onto the MOFs, it might react with the metal nodes and cause hydrolysis. To follow the hydrolysis paths from a kinetics perspective, we focused on the MOF cluster models shown in Fig. S3 and the reaction of the first water molecule (i.e., one axial water in the case of HKUST-1 and MIL-127 and a guest molecule for UMCM-1 and MOF-303). As suggested by hydrolysis pathways R1 and R2, the reactions involve local metal–ligand bond cleavage within the immediate coordination sphere of the metal center. To confirm this and validate the adequacy of the MOF clusters (Fig. S3) for kinetics studies, we carried out density of states (DOS) and Fukui analyses[44] on the extended MOF clusters before and after water adsorption (Fig. S1 and S2). The DOS profiles are presented in Fig. S4, and they reflect the role of adsorbed water in redistributing the cluster's states. Based on the changes in the peak positions and intensities of the DOS profiles, the addition of water alters the distribution of states around the frontier orbitals of HKUST-1(triplet), MIL-127(Fe) and UMCM-1. For MOF-303, major changes take place in the states further from the valence orbitals. All these changes indicate the electronic activity of the clusters (and their structural relaxations), in the presence of guest water molecules. In the case of HKUST-1 (in the singlet state), a minimal electronic perturbation is observed, highlighting the lower electronic (and structural) activity of the closed-shell antiferromagnetic singlet state, relative to the open-shell triplet state.

After confirming the electronic activity of the models, the active sites for hydrolysis were identified using the Fukui index

This journal is © the Owner Societies 2026

Phys. Chem. Chem. Phys., 2026, 28, 6089–6098 | 6093

for nucleophilic reactions (f^+), which goes beyond frontier orbital analysis by assessing the impact of electron addition and, therefore, the susceptibility of an atom toward nucleophilic attack. The larger the absolute f^+ index, the higher the activity and nucleophilic attack susceptibility.[45] The f^+ indices calculated through Hirshfeld atomic charges[46] of the MOF clusters with 0 to 10 adsorbed water molecules (Fig. S1 and S2) in the presence and absence of an additional electron are reported in Tables S2–S6.

In both singlet (Table S2) and triplet (Table S3) states, the Cu atoms of the HKUST-1 clusters with varying water contents show the highest $|f^+|$ values, declaring the metal centers as the main active site for hydrolysis. The carboxylate oxygens and the carbon atoms attached to them also present some level of activity. Similarly, the Fe atoms of MIL-127(Fe) (Table S4) with the highest $|f^+|$ values demonstrate high nucleophilic activity. In this cluster, the oxygen bridging between the Fe atoms (indexed as O202) also shows outstanding activity and the carbon atoms attached to the carboxylate oxygens present significant activities. The main activity center shifts from the metals to a ligand in MOF-303 (Table S5). The Al atoms of MOF-303 are associated with insignificant Fukui values ($|f^+| \leq 0.01$), establishing their insusceptibility to hydrolysis. Instead, a ligand located at the edge of the model shows high $|f^+|$ values, particularly its nitrogen atoms (indexed as N129 and N130), carboxylate oxygens (O60, O101 and O160) and carbons (C60, C66, C113 and C114). In UMCM-1 (Table S6), the carboxylate

oxygens and their connecting carbon atoms show higher susceptibility to hydrolysis, relative to the Zn atoms. Therefore, all Fukui indices declare localization of the active sites on the metal nodes of HKUST-1, MIL-127(Fe) and UMCM-1 and a minimally constrained ligand in MOF-303. Therefore, the selected MOF models, depicted in Fig. S3, are adequate for studying the hydrolysis mechanisms, qualitatively.

We note, however, that the size of the models influences the steric environment of metal nodes and their accessibility. Our preliminary tests using the larger fragments of UMCM-1 and MIL-127 (Fig. 1) showed that the (unrestrained) extended ligands can undergo undesired reorientation, hydrogen bonding, or partial collapse upon water addition, which biases the reaction pathways. For instance, the extended UMCM-1 model exhibited substantial ligand–ligand rearrangements after water adsorption. Moreover, larger cluster-based or periodic models significantly increase the computational cost. Therefore, we adopted the smaller UMCM-1-sm model, which avoids these artifacts and isolates the chemically relevant local environment. The resulting PES shown in Fig. 3 is thus more representative of the intrinsic hydrolysis chemistry than those obtained from the larger unconstrained clusters.

According to Fig. 3, UMCM-1 adsorbs the first water molecule to form the INT0 structure, which is 25.2 kJ mol^{-1} more stable than the reactants. This path is simply an association reaction and, therefore, barrierless. The adsorbed water can slightly move, pass through the TS0 barrier (Gibbs free energy
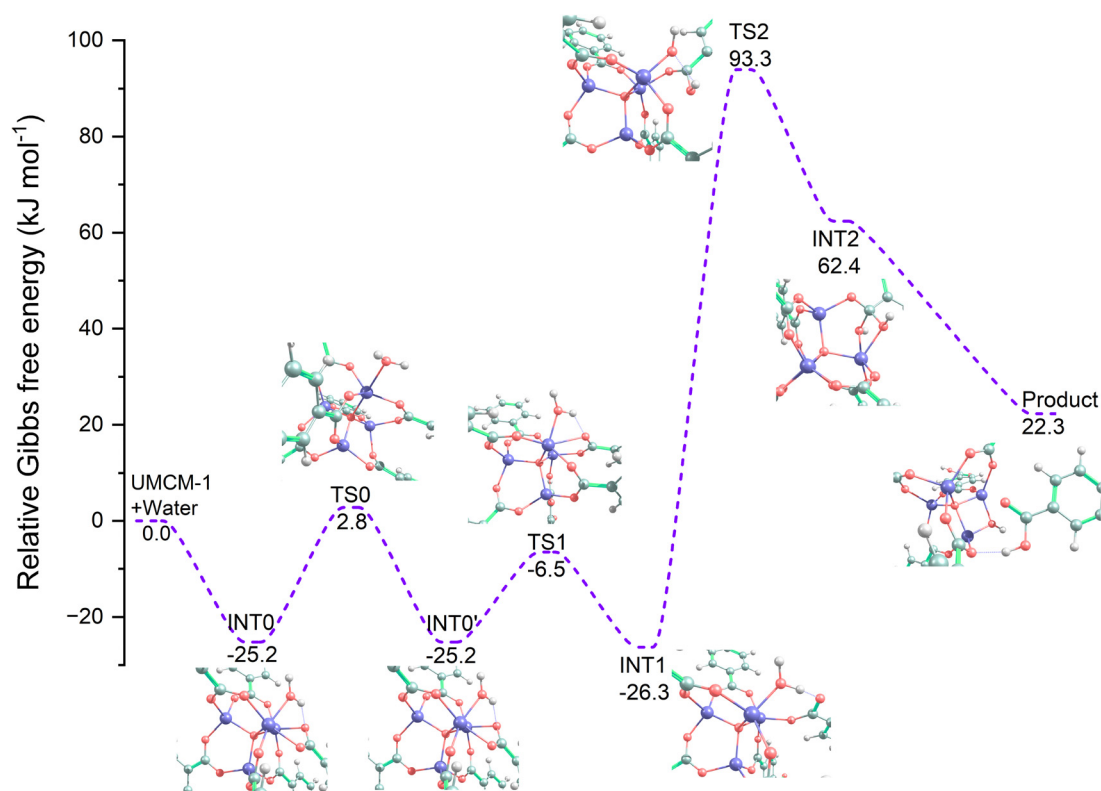

Fig. 3 The potential energy surface of the UMCM-1-sm (smaller model) reaction with one water molecule, at 298.15 K and 1 atm. The species structures are shown in their best views, focusing on the reaction center. The purple, red, grey and white balls represent the Zn, O, C and H atoms, respectively.

6094 | *Phys. Chem. Chem. Phys.*, 2026, **28**, 6089–6098

This journal is © the Owner Societies 2026

relative to reactants: 2.8 kJ mol^{-1}), and face another ligand. However, due to the symmetry imposed by the metal node, the transition does not induce any significant energy or structural changes. After that, the interaction of the water's hydrogen atom and the carboxylate oxygen (Oc) causes gradual elongation of the metal–Oc bond and water–metal axis distortion toward the ligand (changing the geometry of the water-attached Zn from tetrahedral to pyramidal). These changes induce some strain as Zn^{2+} prefers a tetrahedral arrangement in many systems (such as zeolites)[47,48] but can also exist in a square pyramidal state in MOFs.[49,50] As a result of the changes, a ligand detaches from one Oc end and water takes the Oc's position in the metal's coordination space, giving INT1 (−26.3 kJ mol^{-1}). This reaction step (reaction (R2) according to the "Introduction") is kinetically favorable because the associated TS (TS1: −6.5 kJ mol^{-1}) has an energy lower than the reactants and the energy conserved in INT0/INT0′ is sufficient for supporting the transition.

The next step (reaction (R2)) involves a barrier (TS2) that is 93.3 kJ mol^{-1} above the reactants. Consequently, the INT1 to product path is both kinetically and thermodynamically unfavorable. If enough energy is supplied by the environment, one hydrogen atom will transfer from the water to the metal-bound Oc atom, facilitating the detachment of the ligand from both its Oc sides and replacing the ligand with a metal–metal bridging OH moiety, as the final product. In the product, the ligand still interacts with the metal node through hydrogen bonding.

Alternatively, the presence of other species, such as other water molecules, might lower the barrier. This possibility was not evaluated in our work. But, according to a study on MOF-5 (IRMOF-0h) (which has tetrahedral Zn$_4$O metal centers and terephthalic acid (BDC) linkers, rather similar to the UMCM-1-sm model), the increase of water content in the pores and the co-adsorption of water molecules in the vicinity of the metal node lower the barrier to Zn–Oc bond cleavage to around 4 kJ mol^{-1} (at 300 K) and make the reaction more exothermic.[35] Regardless of the factors controlling the INT1 to product path, the INT1 generation is intrinsically kinetically and thermodynamically feasible. Therefore, one water molecule is enough to destabilize UMCM-1. That is why UMCM-1 is experimentally observed to be highly unstable.[8]

In the case of HKUST-1, the reaction mechanisms are not as simple as UMCM-1's PES. The model can be in both singlet and triplet states. Based on our model-based (condensation) calculations, the triplet state is over 100 kJ mol^{-1} more stable regardless of the number of guest water molecules (Table S7). This was further validated by performing single-point energy calculations on the optimized cluster model at the M06-2X/LanL2DZ/GD3, HSE06/6-31+G* and PBE0/Def2-TZVP/GD3 levels. However, preliminary periodic calculations on HKUST-1 (with no axial water molecules) with fully paired metal node electrons (singlet) and two unpaired electrons on each metal node (triplet) showed that the singlet state is 51.6 kJ mol^{-1} more stable than the triplet state. The discrepancy between the periodic and cluster models originates from the weak antiferromagnetic coupling between the Cu centers ($S = 1/2$). In the periodic system, the coupling and long-range superexchange through the organic linkers (and facilitated by the high symmetry of the paddle wheels) lead to a singlet ground spin state ($S = 0$).[25] However, the truncation of the MOF and the loss of the superexchange in the cluster models favor delocalization of magnetic coupling, stabilizing the cluster in a triplet state. The weak coupling implies that hydrolysis and other environmental conditions might induce electronic surface crossing for HKUST-1, potentially affecting the reaction barriers.

Herein, we do not compare absolute singlet–triplet splitting between the cluster and periodic models. Instead, we compute the hydrolysis pathways using specific spin states for the cluster model, ensuring internal consistency. Following the work of Xue et al.[26] and their proposed reaction mechanism, we first focused on the singlet state and then evaluated alternative pathways. Based on the observed PES (Fig. 4), the interaction of water's hydrogen with the Oc of a ligand improves as an axial water tilts toward the ligand. This induces the repositioning of the ligand and a change in the coordination geometry of the Cu center to yield hk-INT1 with a relative Gibbs free energy of −13.9 kJ mol^{-1}. The barrier (hk-TS1) is 26.8 kJ mol^{-1} above the reactants. After this step (i.e., reaction (R2)), no transition state was confirmed by IRC analysis on the singlet and triplet surfaces, including the structure reported by Xue et al.[26] This can be either because of the absence of a barrier between hk-INT1 and the hk-product or a very high barrier that is challenging to locate using energy minimizations. Regardless, the proposed hk-product is stable (−10.4 kJ mol^{-1}) and hk-TS1 is higher in energy relative to TS0 of UMCM-1, suggesting the

HKUST-1: 0.0 ⟹ **hk-TS1:** 26.8 ⟹ **hk-INT1:** -13.9 ⤏ **hk-product:** -10.4
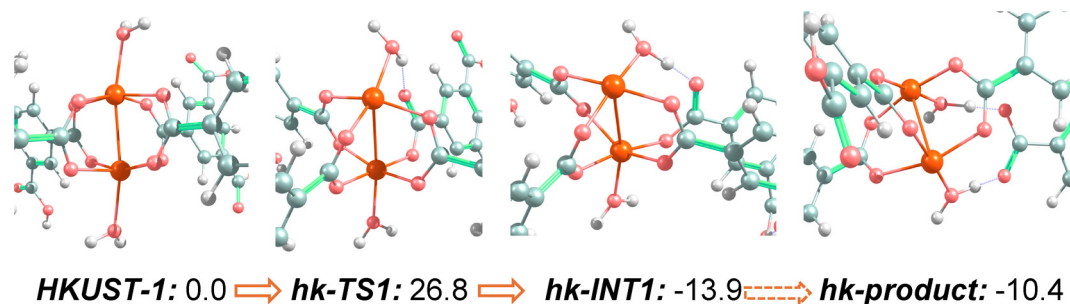
Fig. 4 The hydrolysis reaction path of singlet HKUST-1 initiated by its axial water and the corresponding relative Gibbs free energies, at 298.15 K and 1 atm (in kJ mol^{-1}). The species structures are shown in their best views, focusing on the reaction center. The orange, red, grey and white balls represent the Cu, O, C and H atoms, respectively.

This journal is © the Owner Societies 2026

Phys. Chem. Chem. Phys., 2026, 28, 6089–6098 | 6095

higher stability of HKUST-1 but feasible hydrolysis, in agreement with experimental stability classifications.[8]

When there are guest water molecules, new reaction paths become accessible. We did not follow the reaction in the presence of guest water. However, based on the electron paramagnetic resonance spectroscopy (EPR) performed by Todaro et al.,[25] the accumulation of a large amount of water inside HKUST-1 pores enforces reversible Cu–Cu σ-bond formation and triplet to singlet state change, evidenced by loss of an EPR peak. This change is the direct impact of the weak coupling of the Cu centers, as aforementioned. Considering the condensation energy and geometry results summarized in Table S7, the singlet geometries show a shorter Cu–Cu bond length, relative to their triplet counterparts. However, as aforementioned, the triplet state remains more stable in the cluster model because of the loss of superexchange after HKUST-1 truncation, and the Cu–Cu bond length does not reduce with water uptake. For all triplet structures, the total spin eigenvalue is 2.00, indicating no spin contamination biasing our energy results. As our model-based results contrast such a spin state change but the periodic calculations declare higher stability of the singlet state, we believe that the spin state change is an impact of long-range superexchange with other metal nodes rather than the influence of localized water clusters.

When in the singlet state, one of the Cu^{2+} atoms reduces to Cu^+ in some metal nodes, replacing residual E″(Cu) EPR peaks with E′1(Cu) centers and giving a doublet metal node.[25] Todaro et al.[25] considered this as a result of Cu–Oc hydrolysis. Based on our analysis of doublet HKUST-1 models (Table S8 and Fig. S5), the redox process is not necessary for hydrolysis and ligand detachment. However, the doublet state facilitates the Cu–Oc bond cleavage. Therefore, the presence of reducing agents enhances the rate of hydrolysis. Notably, in the singlet state, the average charge of the two Cu atoms is 1.14 C (vs. 1.74 C for triplet and 0.64 for Cu^+ in the doublet state), which reduces to 0.85 C for hk-TS1. Therefore, we believe that Cu^{2+} to Cu^+ reduction does not precede hydrolysis. It is merely an outcome of the singlet state and hydrolysis.

The hydrolysis process proposed by Todaro et al.[25] continues from an intermediate and a transition state similar to hk-INT1 and hk-TS to a charge-balanced structure with a detached protonated ligand, an OH moiety filling the detached Oc position and a second axial water that faces and removes the second Oc of the detaching ligand (in the doublet state).

Moving from HKUST-1 to MIL-127, we observe a reaction mechanism (Fig. 5) similar to that of singlet HKUST-1 (Fig. 4). An axial water molecule approaches the direction of a carboxylate ligand while its hydrogen interacts with the ligand's Oc to separate it from Fe and re-adjust the water's position in the Fe's coordination shell. This reaction path (R1) passes through the high barrier of mi-TS1 (47.6 kJ mol^{-1}) to give mi-INT1 (29.3 kJ mol^{-1}). Therefore, the path is kinetically infeasible and thermodynamically non-spontaneous. As in the case of HKUST-1, no further path was confirmed by IRC analysis. Moreover, the proposed final product, mi-product, is 51.1 kJ mol^{-1} less stable than the reactants. The higher barrier of mi-TS1, with respect to hk-TS1 and TS1, and the thermodynamic infeasibility explain the higher hydrolytic stability of MIL-127 relative to HKUST-1 and UMCM-1.[8] We found no experimental or computational data to evaluate the possibility of hydrolysis facilitation by water condensation in MIL-127 pores.

In the case of MOF-303, which is known for its outstanding hydrolytic stability,[8] we observed no confirmed transition state using any of the models shown in Fig. S3. All guessed transition states stabilized by pushing water away from Al atoms and stabilizing the guest water through hydrogen bonding, consistent with the Fukui results in Table S5. In some guessed structures, the water ended up interacting with terminal (unrestricted) ligands and capped OH/H_2O moieties. In some others, water stabilized in the space between the metal center and the ligands.

Aluminum, especially in aqueous solutions, prefers the Al^{3+} oxidation state,[51] as in the MOF-303 structure. Therefore, we do not suspect any potential changes in the oxidation state of Al in MOF-303. Moreover, Al–O bonds are not intrinsically hydrolysis resistant. For example, Al–O bonds in some zeolites undergo hydrolysis.[52] Therefore, we believe that the water stability of MOF-303 is because of the ligands, which facilitate many stabilization routes using hydrogen bonding. This is supported by our observation of many water-framework interaction modes

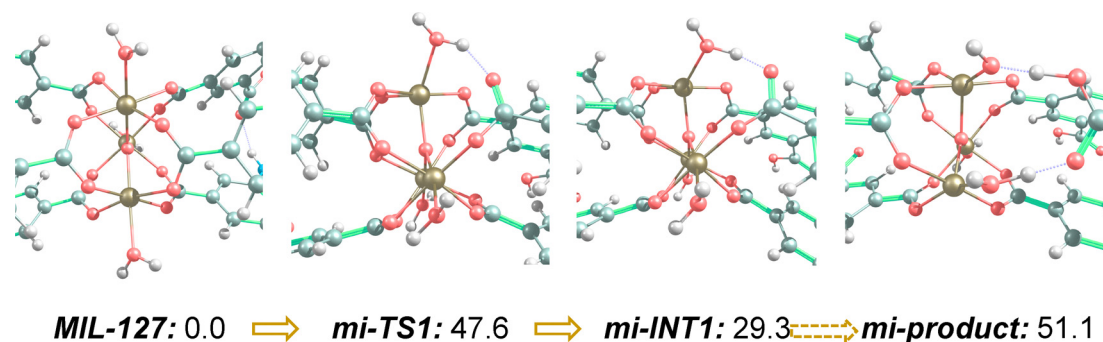**MIL-127:** 0.0 ⟹ **mi-TS1:** 47.6 ⟹ **mi-INT1:** 29.3 ⤏ **mi-product:** 51.1

Fig. 5 The hydrolysis reaction path of MIL-127 initiated by its axial water and the corresponding relative Gibbs free energies, at 298.15 K and 1 atm. The species structures are shown in their best views, focusing on the reaction center. The dark yellow, red, grey and white balls represent the Fe, O, C and H atoms, respectively.

6096 | Phys. Chem. Chem. Phys., 2026, **28**, 6089–6098

This journal is © the Owner Societies 2026

during molecular dynamics simulations on periodic MOF-303 and the distribution of water molecules throughout the MOF-303 structure during the condensation process (Fig. S1). As more water molecules enter MOF-303 pores, the extended hydrogen bonding network harnesses their movement and stabilizes them. This prevents them from approaching the metal-center and breaking the Al–O bonds, which increases the barrier to hydrolysis to an extent that the barrier's allocation becomes extremely challenging. Simultaneously, as aforementioned in discussing the water condensation process, the extended water–ligand hydrogen bonding network prevents (even the unrestrained) ligands from collapsing on each other. Therefore, the cooperation of the water molecules and the ligands through hydrogen bond networking establishes water stability. This is in contrast to the case of the other MOFs with relatively hydrophobic ligands, in which water condensation enforces spin and oxidation state changes (HKUST-1) or directly lowers the barrier to hydrolysis by intensifying water–water interaction with carboxylate ligands (UMCM-1). Therefore, hydrophobicity does not necessarily improve water stability, in contrast to the general belief.[9–11] When combined with denser connectivity of metal nodes, as in MOF-303, hydrophilicity can provide superior water stability.

Furthermore, we note that the other general features outlined in the "Introduction" as indicators of higher water stability might be contrasted by some MOFs. For instance, Al (in MOF-303) has an ionization potential of 5.986 eV,[53] which is lower than the 7.5 eV limit suggested as a stability criterion.[23] Zn (in UCMC-1) has an atomic radius of 1.39 Å,[54] very close to the 1.4 Å limit,[23] and a Pauling electronegativity of 1.65 that is 0.04 higher than the electronegativity of Al. Both are connected to oxygen in their MOFs, one highly stable and one highly unstable. Therefore, they do not follow the high electronegativity difference guideline.[22] In other words, no specific guideline correctly describes all MOFs and their stabilities.

3. Conclusions

This study demonstrates a comparative molecular picture of water adsorption, condensation, and hydrolysis in four prototypical MOFs with distinct water stabilities. We find that while open metal sites govern the onset of water adsorption, the hydrolysis and the subsequent steps of water uptake and condensation depend strongly on framework properties. In particular, hydrogen-bond networks between water and ligands can protect metal–oxygen bonds, as in MOF-303, by stabilizing water molecules and restricting their access to the metal–oxygen bonds. However, π-stacking of ligands detached after hydrolysis and their hydrogen bonding in the presence of water accelerate water-induced structural collapse, as in UMCM-1. Moreover, hydrogen bonding of water and the pressure of the condensed phase can induce geometrical, spin and redox state changes to facilitate hydrolysis, as in HKUST-1. Our results highlight contradictions in existing heuristic guidelines and show that no single descriptor (e.g., hydrophobicity or metal–ligand electronegativity difference) reliably predicts stability

across MOFs. They also indicate that strong water adsorption does not align with high water stability, as both highly stable MOF-303 and highly unstable UMCM-1 models show strong water adsorption. Instead, cooperative effects between metal connectivity, ligand hydrophilicity, and framework rigidity govern hydrolytic resilience. These insights not only clarify degradation pathways in representative MOFs but also provide transferable design principles to guide the development of robust materials for aqueous-phase and moisture-rich applications.

Conflicts of interest

There are no conflicts to declare.

Data availability

All data supporting this article have been included as part of the submitted manuscript and the supporting information (SI). Supporting information: computational details (Section S1); adsorption modes of the MOF model–water clusters (Fig. S1 and S2); their corresponding energies (Table S1); models used for reaction kinetics explorations (Fig. S3), structural, charge and energy profiles of the HKUST-1 model in different spin states (Tables S2 and S3); the associated structures (Fig. S4); and the optimized structures (SI-structures.zip). See DOI: https://doi.org/10.1039/d5cp04782j.

Acknowledgements

References

1 J. Liu, G. Xing and L. Chen, *Acc. Chem. Res.*, 2024, **57**, 1032–1045.

2 E. A. Dolgopolova, A. J. Brandt, O. A. Ejegbavwo, A. S. Duke, T. D. Maddumapatabandi, R. P. Galhenage and B. W. Larson, *et al.*, *J. Am. Chem. Soc.*, 2017, **139**, 5201–5209.

3 S. Wang, W. Morris, Y. Liu, C. M. McGuirk, Y. Zhou, J. T. Hupp, O. K. Farha and C. A. Mirkin, *Angew. Chem., Int. Ed.*, 2015, **54**, 14738–14742.

4 M. Ranocchiari and J. A. van Bokhoven, *Phys. Chem. Chem. Phys.*, 2011, **13**, 6388–6396.

5 A. J. Emerson, C. S. Hawes, M. Marshall, G. P. Knowles, A. L. Chaffee, S. R. Batten and D. R. Turner, *Chem. Mater.*, 2018, **30**, 6614–6618.

6 W. Li, P. Xu, Z. Wang, Y. He, H. Qin, Y. Zeng, Y. Li, Z. Zhang and J. Gao, *Mater. Chem. Front.*, 2023, **7**, 5140–5170.

7 Z. Zheng, N. Hanikel, H. Lyu and O. M. Yaghi, *J. Am. Chem. Soc.*, 2022, **144**, 22669–22675.

8 N. C. Burtch, H. Jasuja and K. S. Walton, *Chem. Rev.*, 2014, **114**, 10575–10612.

This journal is © the Owner Societies 2026

Phys. Chem. Chem. Phys., 2026, **28**, 6089–6098 | **6097**

9 M. J. Kalmutzki, C. S. Diercks and O. M. Yaghi, *Adv. Mater.*, 2018, **30**, 1704304.

10 J. J. Low, A. I. Benin, P. Jakubczak, J. F. Abrahamian, S. A. Faheem and R. R. Willis, *J. Am. Chem. Soc.*, 2009, **131**, 15834–15842.

11 K. Yang, T. Pan, Q. Lei, X. Dong, Q. Cheng and Y. Han, *Environ. Sci. Technol.*, 2021, **55**, 6542–6560.

12 T. A. Makal, X. Wang and H.-C. Zhou, *Cryst. Growth Des.*, 2013, **13**, 4760–4768.

13 X. Zhang, B. Wang, A. Alsalme, S. Xiang, Z. Zhang and B. Chen, *Coord. Chem. Rev.*, 2020, **423**, 213507.

14 B. Liu, K. Vikrant, K.-H. Kim, V. Kumar and S. K. Kailasa, *Environ. Sci.: Nano*, 2020, **7**, 1319–1347.

15 C. Xiao, J. Tian and M. Hong, *Chem. Sci.*, 2024, DOI: 10.1039/d4sc02158e.

16 M. E. Kosal, J.-H. Chou, S. R. Wilson and K. S. Suslick, *Nat. Mater.*, 2002, **1**, 118–121.

17 C.-Y. Sun, S.-X. Liu, D.-D. Liang, K.-Z. Shao, Y.-H. Ren and Z.-M. Su, *J. Am. Chem. Soc.*, 2009, **131**, 1883–1888.

18 O. Karagiaridi, M. B. Lalonde, W. Bury, A. A. Sarjeant, O. K. Farha and J. T. Hupp, *J. Am. Chem. Soc.*, 2012, **134**, 18790–18796.

19 Z. Lu, H. Xing, R. Sun, J. Bai, B. Zheng and Y. Li, *Cryst. Growth Des.*, 2012, **12**, 1081–1084.

20 L. Liu and S. G. Telfer, *J. Am. Chem. Soc.*, 2015, **137**, 3901–3909.

21 T. Kundu, S. Mitra, P. Patra, A. Goswami, D. Díaz Díaz and R. Banerjee, *Chem. – Eur. J.*, 2014, **20**, 10514–10518.

22 G. G. Terrones, S.-P. Huang, M. P. Rivera, S. Yue, A. Hernandez and H. J. Kulik, *J. Am. Chem. Soc.*, 2024, **146**, 20333–20348.

23 R. Batra, C. Chen, T. G. Evans, K. S. Walton and R. Ramprasad, *Nat. Mach. Intell.*, 2020, **2**, 704–710.

24 D. Yang and B. C. Gates, *J. Phys. Chem. C*, 2024, DOI: 10.1021/acs.jpcc.4c02320.

25 M. Todaro, G. Buscarino, L. Sciortino, A. Alessi, F. Messina, M. Taddei, M. Ranocchiari, M. Cannas and F. M. Gelardi, *J. Phys. Chem. C*, 2016, **120**, 12879–12889.

26 W. Xue, Z. Zhang, H. Huang and D. Mei, *J. Phys. Chem. C*, 2019, **124**, 1991–2001.

27 S. Zhang, Z. Yang, K. Gong, B. Xu, H. Mei, H. Zhang, J. Zhang, Z. Kang, Y. Yan and D. Sun, *Nanoscale*, 2019, **11**, 9598–9607.

28 Y. Ming, N. Kumar and D. J. Siegel, *ACS Omega*, 2017, **2**, 4921–4928.

29 J. A. Greathouse and M. D. Allendorf, *J. Am. Chem. Soc.*, 2006, **128**, 10678–10679.

30 L. Bellarosa, S. Calero and N. López, *Phys. Chem. Chem. Phys.*, 2012, **14**, 7240–7245.

31 W. Xue, J. Wang, H. Huang and D. Mei, *J. Phys. Chem. C*, 2021, **125**, 5832–5847.

32 M. C. Oliver, S. Wang, L. Huang, M. Kasule and Y. Wu, *J. Phys. Chem. C*, 2023, **127**, 6503–6514.

33 C. Chen, Z. Yu, D. S. Sholl and K. S. Walton, *J. Phys. Chem. Lett.*, 2022, **13**, 4891–4896.

34 F. Keshavarz, *Chem. Mater.*, 2023, **36**, 439–449.

35 J. Kubecka, V. Besel, T. Kurtén, N. Myllys and H. Vehkamaki, *J. Phys. Chem. A*, 2019, **123**, 6022–6033.

36 B. Zhang, Z. Zhu, X. Wang, X. Liu and F. Kapteijn, *Adv. Funct. Mater.*, 2023, 2304788.

37 P. Küsgens, M. Rose, I. Senkovska, H. Fröde, A. Henschel, S. Siegle and S. Kaskel, *Microporous Mesoporous Mater.*, 2009, **120**, 325–330.

38 P. M. Schoenecker, C. G. Carson, H. Jasuja, C. J. J. Flemming and K. S. Walton, *Ind. Eng. Chem. Res.*, 2012, **51**, 6513–6519.

39 J. M. Castillo, T. J. H. Vlugt and S. Calero, *J. Phys. Chem. C*, 2008, **112**, 15934–15939.

40 J. Bae, S. H. Park, D. Moon and N. C. Jeong, *Commun. Chem.*, 2022, **5**, 51.

41 V. Loianno, M. Pannico, F. S. Gentile, F. Pascale, G. Mensitieri and P. Musto, *Mater. Today Chem.*, 2023, **30**, 101605.

42 S. Chheda, W. Jeong, N. Hanikel, L. Gagliardi and J. I. Siepmann, *J. Phys. Chem. C*, 2023, **127**, 7837–7851.

43 S. Cong, Y. Yuan, J. Wang, Z. Wang, F. Kapteijn and X. Liu, *J. Am. Chem. Soc.*, 2021, **143**, 20055–20058.

44 N. F. Barrera, J. Cabezas-Escares, F. Munoz, W. A. Muriel, T. Gomez, M. Calatayud and C. Cárdenas, *J. Chem. Theory Comput.*, 2025, **21**, 3187–3203.

45 G. Kang, Y. Cao, Q. Liu, J. Duan, Y. Zhang, F. Kang and Y. Cao, *Adv. Funct. Mater.*, 2025, e22713.

46 F. L. Hirshfeld, *Theor. Chim. Acta*, 1977, **44**, 129–138.

47 Y.-X. Tan, F. Wang and J. Zhang, *Chem. Soc. Rev.*, 2018, **47**, 2130–2144.

48 Z. Zheng, Z. Rong, H. L. Nguyen and O. M. Yaghi, *Inorg. Chem.*, 2023, **62**, 20861–20873.

49 M. J. Manos, E. E. Moushi, G. S. Papaefstathiou and A. J. Tasiopoulos, *Cryst. Growth Des.*, 2012, **12**, 5471–5480.

50 Z.-G. Wang, T. Ding and J. Fei, *Dalton Trans.*, 2023, **52**, 14409–14415.

51 T. Loiseau, C. Volkringer, M. Haouas, F. Taulelle and G. Férey, *C. R. Chim.*, 2015, **18**, 1350–1369.

52 B. H. Wouters, T.-H. Chen and P. J. Grobet, *J. Am. Chem. Soc.*, 1998, **120**, 11419–11425.

53 National Center for Biotechnology Information, PubChem, 2025, Ionization energy in the periodic table of elements, https://pubchem.ncbi.nlm.nih.gov/periodic-table/ionization-energy (accessed August 21, 2025).

54 National Center for Biotechnology Information, PubChem, 2025, Atomic radius in the periodic table of elements, https://pubchem.ncbi.nlm.nih.gov/periodic-table/atomic-radius (accessed August 21, 2025).

6098 | *Phys. Chem. Chem. Phys.*, 2026, **28**, 6089–6098

This journal is © the Owner Societies 2026